IEEE Photonics Journal
An IEEE Photonics Society Publication

Open Access

Employing Higher Order Cladding Modes of Fiber Bragg Grating for Analysis of Refractive Index Change in Volume and at the Surface

Volume 12, Number 1, February 2020

Sankhyabrata Bandyopadhyay
Liyang shao
Mateusz Smietana
Chao Wang
Jie Hu
Guoqing Wang
Wei He
Guoqiang Gu
Yatao Yang

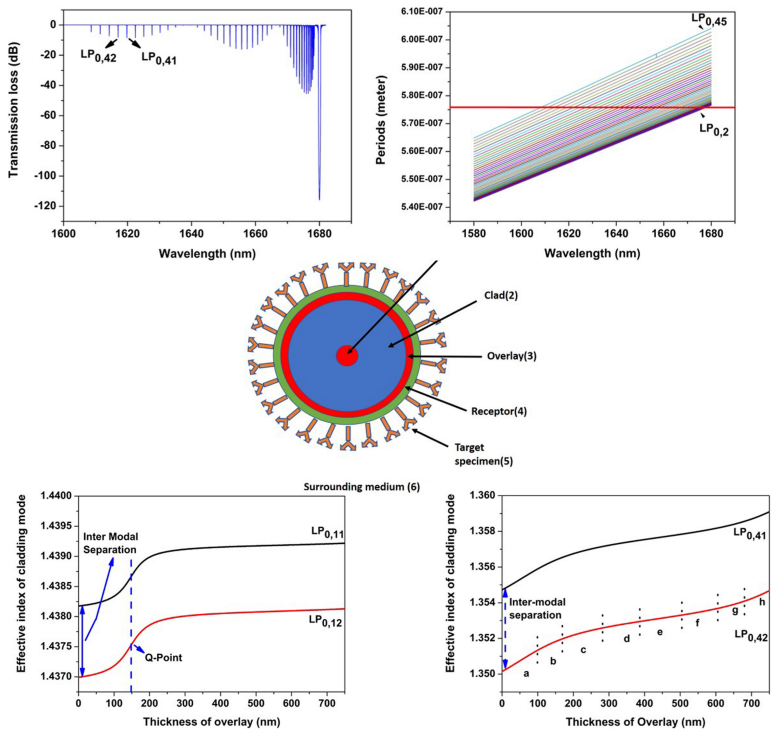

DOI: 10.1109/JPHOT.2019.2963125

Employing Higher Order Cladding Modes of Fiber Bragg Grating for Analysis of Refractive Index Change in Volume and at the Surface

Sankhyabrata Bandyopadhyay,[1] Liyang shao,[1] Mateusz Smietana,[2] Chao Wang,[3] Jie Hu,[1] Guoqing Wang,[1] Wei He,[1] Guoqiang Gu,[1] and Yatao Yang[1]

[1]Department of Electrical and Electronic Engineering, Southern University of Science and Technology, Shenzhen 518055, China
[2]Warsaw University of Technology, Institute of Microelectronics and Optoelectronics, Warsaw 00-662, Poland
[3]School of Engineering and Digital Arts, University of Kent, Canterbury CT27NT, U.K.

DOI:10.1109/JPHOT.2019.2963125

Manuscript received October 19, 2019; revised December 7, 2019; accepted December 25, 2019. Date of publication December 31, 2019; date of current version February 24, 2020. This work was supported by the Startup Fund from the Southern University of Science and Technology and Shenzhen government under Grants Y01236228 & Y01236128, Shenzhen Post Doctoral research grant, Guangdong Basic and Applied Basic Research Foundation under Grant 2019A1515011242, and Shenzhen Postdoctoral Research Grant Program under Grant K19237504. Mateusz Smietana's contribution has been supported in Poland by the National Centre for Research and Development under Grant 347324/12/NCBR/2017. Corresponding author: Liyang Shao (e-mail: liyangshao@gmail.com).

Abstract: In this work, a detailed study on volume and surface refractive index (RI) sensitivity of cladding modes for a fiber Bragg grating (FBG) based sensor is presented. Surface RI sensitivity of the cladding mode of FBGs has been illustrated and quantified with the concept of add-layer sensitivity for the first time to the best of our knowledge. A detailed investigation of mode transition of higher-order cladding modes has been revisited and important characteristics of the cladding modes are observed which could open a new designing path of fabrication and innovative way of the use of this family of optical fiber grating-based sensors. The effect of "mode transition" of higher-order cladding modes, higher operating wavelength for respective cladding mode and "mode stretching" effects are combined together to achieve higher volume and surface RI sensitivity of cladding mode of FBG. It has been shown numerically that with proper designing, sub-nanometer (∼0.04 nm) attachment of target analyte could be recognized by cladding mode of FBG which is quite promising for application in optical fiber grating bio-sensors. This critical designing method of FBG based surface refractometer would be very helpful in case of the fabrication of highly sensitive sensors for distinct biochemical applications.

Index Terms: Fiber Bragg grating, cladding mode, mode transition, surface refractive index sensitivity.

1. Introduction

FBG based sensors were used extensively over the past two decades. Real-time detection scheme, label-free, lightweight and moderate complexity of fabrication make FBG as a potential component for diverse applications [1]–[3]. In FBG, a forward propagating core mode couples with backward

propagating core mode and a particular wavelength of light which is governed by the Bragg reflection law is reflected back to the input end [4]. This reflected wavelength can be changed with external temperature and strain and the shift of the wavelength is mainly governed by electro-optic and strain/mechano-optic coefficients of the fiber [4], [5]. Normally, core mode experiences no interactions with a change in surrounding RI (SRI). However, it can be enhanced significantly with the reduction of the clad diameter [6], [7]. FBG sensors with reduced clad diameter has been used successfully for the detection of chloroform [8], measurement of antigen-antibody interaction [9], DNA-sequencing [10], detection of metal ions [11], chemical gas [12] and in many other bio/chemical applications. The volume RI sensitivity of etched FBG has been risen up to $\sim$300 nm/RIU for the fiber diameter of $\sim$8 μm [8]. With the reduction of clad diameter, the sensitivity can be enhanced significantly but mechanical stability is poor and thus it limits the area of applications and repeated use of the sensor [8], [10]–[12]. Titled FBG (TFBG) was an effective solution to use FBG as a biochemical sensor [3], [13]. In the case of TFBG sensors, the spectrum is very clumsy and the fabrication is also required additional equipment to control the tilt angle of the grating structure. Recently it has been demonstrated numerically that the mode transition of leaky modes of TFBG can be used as a successful refractometer, the detailed numerical computations were employed to analyze the leaky cladding mode of TFBG [14]. The sensitivity of leaky cladding mode was computed and it can be as high as $\sim$5000 dB/RIU and which seems to be very promising but the wavelength based measurement system is always much preferable than measurement of transmission loss with change in SRI. Mode transition (MT) is an effective way for enhancement of sensitivity in the case of cladding mode of long-period fiber grating (LPFG) [15]. An overlay with a RI greater than that of clad material needs to be deposited to initiate the MT and at a particular thickness of the deposited overlay the lowest order cladding mode which possesses the highest energy among the cladding modes is guided by the overlay and effective indices of all other modes are converted to its preceding lower-order cladding mode [15], [16]. The same idea of MT of cladding mode was incorporated in case of symmetric cladding mode of FBG and sensitivity of a particular cladding mode was enhanced significantly with change in SRI near the water medium [17]. In this paper, it has been shown that utilizing the longer wavelength of operation, higher-order cladding mode, MT, mode stretching and higher RI overlay the volume and surface RI sensitivity can be enhanced significantly. The comprehensive understanding of the mechanisms and physicochemical parameters controlling the adsorption behavior is crucial for the development and fabrication of innovative chemical and biosensors. Adsorption behavior of target analyte can be understood clearly with quantification of surface-based changes. Precisely change in dielectric and physical properties around the surface within few tens of nm is utmost important to evaluate the biochemical sensing principle. It has been found that for accurate quantification of captured biochemical analyte at the surface of optical sensors defining add-layer sensitivity is much more essential than that of bulk RI sensitivity of the cladding mode. Surface plasmon resonance (SPR) based sensors, Quartz crystal microbalance (QCM), surface acoustic wave (SAW)-based sensors were used successfully for the quantification of localized surface change as a result of target analyte and receptor attachment during specific biochemical sensors [18]–[20]. Recently, the add-layer sensitivity of LPFG was illustrated elsewhere to quantify the surface-based changes during specific applications [21], [22]. In the case of FBG based sensors till now there are not enough studies are being accomplished for characterization of add-layer sensitivity for surface-based measurement purpose according to our knowledge. Standard fabrication methods, ease of use and reference temperature measurement with Bragg resonance peak give this family of symmetric cladding mode-based FBG refractometric sensors an added advantage than conventional LPFG based sensors. FBG refractometer with symmetric cladding modes has much more mechanical stability than etched FBG sensors as significant etching is not required to fabricate the refractometer. Properly designed FBG based RI sensors can be used in an array of sensors with utilizing multiplexing properties of FBG. In this work, the add-layer sensitivity of different order cladding modes of FBG has been characterized numerically. We have shown that an FBG can be fabricated to support higher-order cladding modes and could be used successfully for surface-based measurements. With a thorough investigation, it has been

found that the behavior of MT of higher-order cladding modes takes place in a different way than comparative lower-order cladding modes. A detail description has been given in this work which leads to a different scope and opportunity of designing cladding modes. The mode stretching effect has been introduced by a nominal reduction of the clad diameter of FBG to enhance the sensitivity further. An enhancement of sensitivity can be achieved with this proposed technique which could be useful for designing and fabrication of biological sensors. In this work, a multi-layer architectural model of FBG was developed to quantify the surface sensitivity of FBG. It has been observed that sub-nanometer attachment of bio-analyte can be quantified with properly designed FBG. The architecture of the paper is as follows. In Section 2, a discussion of basic theory has been illustrated which was used for the computation purpose. Detail numerical works are given in Section 3. Section 4 is devoted to discussion and conclusion of the work.

2. Basic Theory

Coupled mode theory is the basic backbone mechanisms to quantify the coupling of light between core and cladding modes of any waveguide structure. In the case of FBG forward propagating core mode couples with backward propagating core mode and backward propagating cladding modes [23]. Transverse electric field components of the guided core or cladding modes propagating along the z-axis of the fiber gratings can be expressed by a generalized equation (1a) and the radial function $\psi(r)$ of the individual layer of optical fiber can be written as in equations (1b)–(1c). where $k_0 = \frac{2\pi}{\lambda}$ is the free space wavenumber, n is the refractive index of the layer, $\beta_{\nu j}$ is the longitudinal propagation constant of the $LP_{\nu,j}$ mode and $\gamma_{\nu,j} = \sqrt{[k_0^2 n^2 - \beta_{\nu,j}^2]}$ is the magnitude of the transverse wave number. $A_{\nu,j}$ and $B_{\nu,j}$ are the field expansion coefficients determined by the boundary condition of the cylindrical layers. $J_\nu(r\gamma_{\nu,j})$ and $Y_\nu(r\gamma_{\nu,j})$ are the ordinary Bessel function of the first and second kind, while $I_\nu(r\gamma_{\nu,j})$ and $K_\nu(r\gamma_{\nu,j})$ are the modified Bessel function of first and second kind of order ν.

$$\Psi(r,\theta,\phi) = e^{-j\beta_\nu z}\Psi(r)\Theta(\theta)\Phi(\phi) \tag{1a}$$

$$\psi(r) = A_{\nu,j}J_\nu(r\gamma_{\nu j}) + B_{\nu,j}Y_\nu(r\gamma_{\nu j})\beta_{\nu j} < k_0 n \tag{1b}$$

$$\psi(r) = A_{\nu,j}I_\nu(r\gamma_{\nu j}) + B_{\nu,j}K_\nu(r\gamma_{\nu j})\beta_{\nu j} > k_0 n \tag{1c}$$

The optical guided modes in the core are being governed by equation (1a). Equation (1b) is the characteristics equation of the cladding mode. The transfer matrix method [23] has been successfully applied to find out the effective indices of the modes and field expansion coefficients of multi-layer LPFG waveguide structure. Field expansion coefficients of each layer are normalized, so that each mode carries the same power P_0, as in equation (2).

$$P_0 = \frac{\beta_{0j}}{2\omega\mu_0}\int_0^{2\pi} d\Phi \int_0^{\infty} \psi(r)\psi^*(r) r dr \tag{2}$$

2.1 Coupled Mode Theory for FBG

A detail calculation of mode coupling characteristics between core and cladding modes of FBG has been carried out for a multi-layer step-index fiber geometry as shown in Fig 1. In this work, coupled-mode equations have been solved numerically with standard differential equations, as a boundary value problem in accordance with the guiding properties of FBG. Mode coupling equations for FBGs were considered as [4], [23]

$$\frac{dA^{co}}{dz} = ik_{01-01}^{co-co}A^{co} + i\frac{m}{2}k_{01-01}^{co-co}B^{co}\exp(-i2\delta_{01-01}^{co-co}z) + \sum_\nu i\frac{m}{2}k_{0\nu-01}^{cl-co}B_{o\nu}^{cl}\exp(-i2\delta_{0\nu-01}^{cl-co}z) \tag{3}$$

$$\frac{dB^{co}}{dz} = -ik_{01-01}^{co-co}B^{co} - i\frac{m}{2}k_{01-01}^{co-co}A^{co}\exp(-2i\delta_{01-01}^{co-co}z) \tag{4}$$

$$\sum_\nu \frac{dB_{0\nu}^{cl}}{dz} = -i\frac{m}{2}k_{0\nu-01}^{cl-co}A^{co}\exp(-i2\delta_{0\nu-01}^{cl-co}) \tag{5}$$

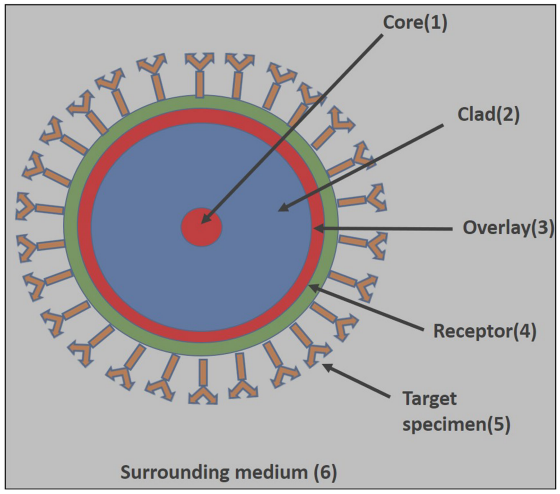

Fig. 1. Multilayer cross-sectional structure of proposed FBG.

where A^{co} and B^{co} represents the amplitudes of forward and backward propagating core modes respectively. The term 'm' is the induced modulation. $B^{cl}_{0,\upsilon}$ is the amplitude of the backward propagating cladding modes of order υ. k^{co-co}_{01-01} is the self-coupling coefficient between forward propagating core and backward propagating core mode. $k^{cl-co}_{0,\upsilon-01}$ are the cross-coupling coefficients between forward propagating core mode (LP_{01}) and backward propagating cladding modes ($LP_{0\upsilon}$). δ^{co-co}_{01-01} and $\delta^{cl-co}_{0\upsilon-01}$ are the detuning parameters and can be represented as

$$\delta^{co-co}_{01-01} = \frac{1}{2}\left(2\beta^{co}_{01} - \frac{2\pi}{\Lambda}\right) \tag{6}$$

$$\delta^{cl-co}_{0\nu-01} = \frac{1}{2}\left(\beta^{co}_{01} + \beta^{cl}_{0\nu} - \frac{2\pi}{\Lambda}\right) \tag{7}$$

Detuning parameters describe the departure from the phase-matching condition. β^{co}_{01} and $\beta^{cl}_{0\upsilon}$ are the propagation constants of forward propagating core mode and backward propagating cladding mode, respectively. Coupling coefficients were computed using the following equation

$$k_{0\nu,0k} = \int_{\Phi=0}^{2\pi} d\Phi \int_{r=0}^{\infty} \Delta\varepsilon\psi_{0\nu}(r)\psi_{0k}(r)rdr \tag{8}$$

where $\psi_{0\upsilon}$ and ψ_{0k} are the radial field components of $LP_{0\nu}$ and LP_{0k} modes. $\Delta\varepsilon$ is the permittivity variation and for this particular waveguide problem, is defined as $2\varepsilon n\Delta n$, where Δn is the induced change in RI of the core during inscription of grating. During the theoretical study, it has been observed that dealing three-layer FBG model with hybrid mode analysis is a very tedious process and designing of multi-layer model of FBG with hybrid modes is very difficult. A numerical model with transfer matrix method [23]–[25] was developed to understand modal coupling for LPFG with linear polarize modes approximation, this technique has been adopted here for numerical modeling of FBG. This approximation was found useful because the model can be extended up to multilayered architecture by modifying the fundamental equations. Effective indices of cladding mode have been calculated with the transfer matrix method [23]. After evaluation of effective indices and the propagation constants of core and cladding modes, amplitudes of the core and cladding modes, self and cross-coupling coefficients between the counter-propagating core and cladding modes along with detuning parameters were also evaluated subsequently with the developed numerical model. With these results, a matrix representing a set of coupled differential equations describing the FBG with an overlay layer was formulated, which is given in equation (9). The system

matrix can be represented as

$$\begin{pmatrix} \frac{dA^{co}}{dz} \\ \frac{dB^{co}}{dz} \\ \frac{dB^{cl}_{02}}{dz} \\ . \\ . \\ \frac{dB^{cl}_{0\nu}}{dz} \end{pmatrix} = \begin{pmatrix} S & \frac{m}{2}S^{co-co} & \frac{m}{2}S^{cl-co}_{02-01} & . & . & \frac{m}{2}S^{cl-co}_{0\nu-01} \\ -\frac{m}{2}S^{co-co} & -S & 0 & . & . & 0 \\ -\frac{m}{2}S^{cl-co}_{02-01} & 0 & 0 & 0 & 0 & 0 \\ . & . & . & . & . & . \\ . & . & . & . & . & . \\ -\frac{m}{2}S^{cl-co}_{0\nu-01} & 0 & 0 & 0 & 0 & 0 \end{pmatrix} \begin{pmatrix} A^{co} \\ B^{co} \\ . \\ . \\ . \\ B^{cl}_{0\nu} \end{pmatrix} \tag{9}$$

where S, S^{co-co}, and $S^{cl-co}_{0\nu-01}$ are defined as

$$S = ik^{co-co}_{01-01} \tag{10}$$

$$S^{co-co} = ik^{co-co}_{01-01}\exp(-i2\delta^{co-co}_{01-01}z) \tag{11}$$

$$S^{cl-co}_{0\nu-01} = ik^{cl-co}_{0\nu-01}\exp(-i2\delta^{cl-co}_{0\nu-01}z) \tag{12}$$

The transmission spectrum was computed by solving the boundary value problem differential equations for each of the cladding modes. Boundary conditions state that all the cladding modes $B^{cl}_{0\nu}$ vanish at the end of the grating length. Numerical computations were carried out by solving the boundary value problem as defined by equation (9). MATLAB software was used for simulating the results.

2.2 Volume and Surface Change

The volume RI sensitivity of a particular cladding mode is defined as a change in resonance wavelength with respect to the surrounding refractive index change. If change in resonance wavelength is defined as $\Delta\lambda_{resonance}$ and change in surrounding RI by Δn then the volume or bulk RI sensitivity is defined as $S_v = \frac{\Delta\lambda_{resonance}}{\Delta n}$, where S_v is defined as the volume or bulk RI sensitivity.

Surface-based changes can be occurred by two ways: 1) adsorption of mass of the biochemical analyte over the specific receptor layer which can be quantified by change in resonance wavelength $\Delta\lambda_{resonance}$ of a particular cladding mode with respect to thickness of a bio-analyte layer (depends on the deposited mass over the surface of the sensors) while the RI property of surrounding medium is remaining same and 2) A change in RI of the receptor layer after interaction with specific target analytes without altering the RI of the surrounding medium. The detailed quantification of these surface-based changes with "add-layer sensitivity" was described elsewhere [21], [22].

Add-layer sensitivity can be defined as in equation below: consider t_{BL} is the thickness of the added bio-layer and n_{BL} is the corresponding RI of the biochemical layer. S_{th} is defined as a change of resonance wavelength of cladding mode with adsorption of thin protein layer and S_{LRI} is the change in resonance wavelength with the change in RI of few tens of nm layer very near to the surface of the sensors with keeping the same surrounding RI.

$S_A = \frac{d\lambda_{resonance}}{dt_{BL}} + \frac{d\lambda_{resonance}}{dn_{BL}} = S_{th} + S_{LRI}$, development of a multilayer FBG model for bio/chemical sensors has been discussed in this paper and would be able to quantify the adsorption of analyte bio-molecules with optimal sensitivity. Investigation of the add-layer sensitivity of FBG cladding mode with a multilayer model has been proposed for the first time to the best of our knowledge.

3. Numerical Results

The fiber geometry and the refractive indices of the core and the cladding material were considered to be that of a standard single-mode fiber SMF 28 of Corning Inc. Selected core diameter for computation purpose was $\sim$9 μm and diameter of the the fiber was $\sim$125 μm. Refractive indices of the core and the cladding material were considered to be 1.4494 and 1.444, respectively. The index modulation was taken as 0.0003, length of the grating was 25 mm and period of the grating was taken as 0.5313 μm. Spectrum was computed with the surrounding medium as air. Computed

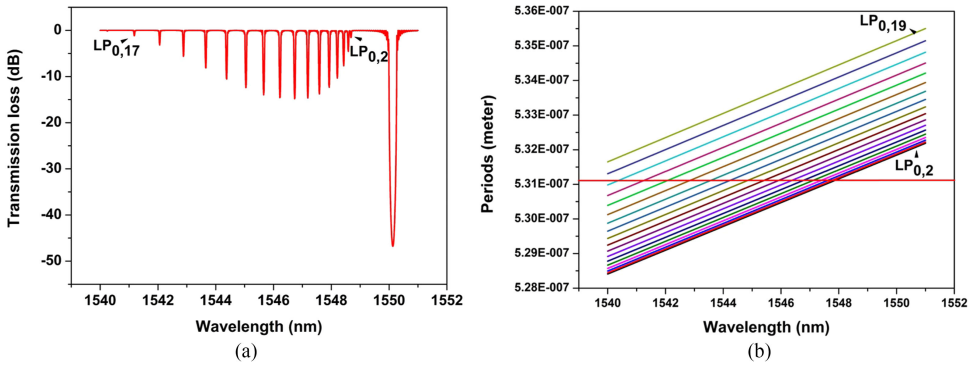

Fig. 2. (a) The computed spectrum of FBG with the first 17 cladding mode and (b) simulated phase plot for the first 17 lower-order cladding modes.

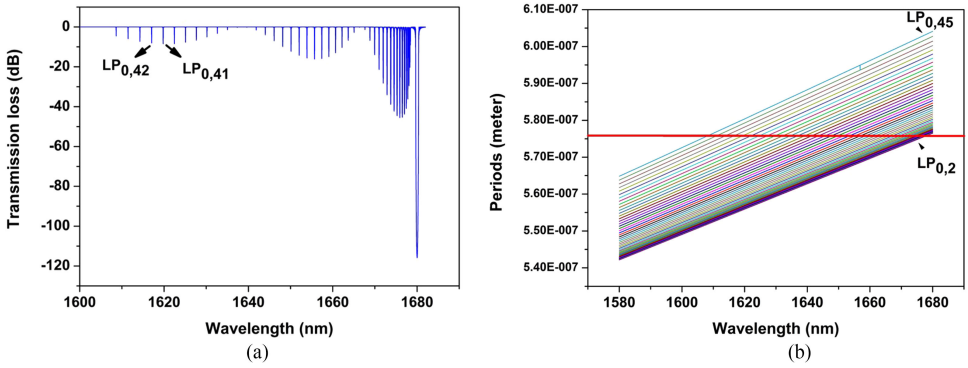

Fig. 3. (a) Computed spectrum of FBG with 45 cladding mode and (b) simulated phase plot for 45 cladding modes.

transmission spectrum along with phase plot of respective cladding modes are being plotted in Fig. 2(a) and Fig. 2(b) respectively. The horizontal red line in Fig. 2(b) represents the grating period, it is to be known that the cross-section points of this horizontal lines with the phase curve of cladding modes determines the position of the resonance wavelength of the respective cladding modes. A detail investigation of volume RI sensitivity of cladding mode was reported earlier. In this previous work, the sensitivity of the respective cladding modes was enhanced with the effect of mode transition and mode stretching [26]. Sensitivity can be enhanced further by adjusting the operating wavelength of cladding mode at higher resonance wavelength which was illustrated earlier in case of long-period fiber sensors. In the next part of the simulation, the period of the grating has been changed to $\sim$0.576 μm, to find a Bragg resonance wavelength peak at $\sim$1680 nm. The sensitivity of cladding mode can be enhanced by using a higher-order cladding mode. If we can change the modulation index of RI higher than $\sim$0.0003, then respective higher-order cladding modes could be observed in the spectrum and which might be used for the sensing applications. In the case of FBG, we can generate an observable higher order of cladding modes with a higher index of modulation. With a modulation (Δn) of $\sim$0.0007, almost 45 cladding modes are being observed in the shorter wavelength side of the main Bragg resonance dip in the computed spectrum, Fig. 3(a) shows the computed spectrum of FBG with Bragg transmission wavelength at $\sim$1680 nm. The respective phase plots of the cladding modes are being given in Fig. 3(b). With this approach a considerably higher order cladding modes could be used for the sensing applications; aim is to revisit the sensitivity of these higher-order cladding modes and to analyze the behavior of transition of modes. Numerically computed spectrum of FBG with different index modulation is being depicted in Fig. S1. in the supplementary document. The simulated spectrum of FBG with

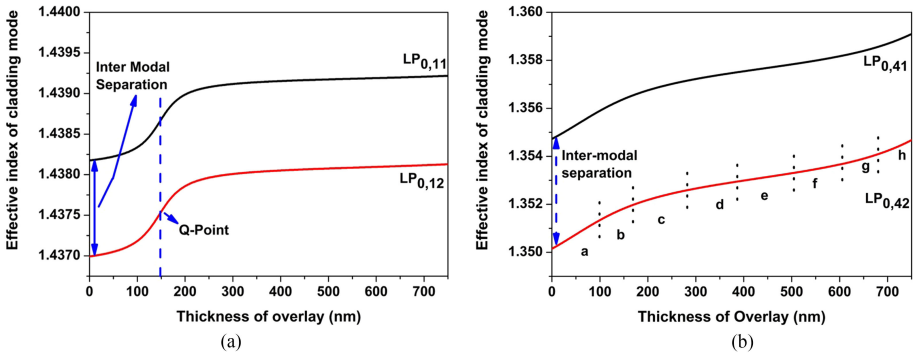

Fig. 4. (a) Variation of effective index of cladding modes with deposition of overlay for $LP_{0,11}$ and $LP_{0,12}$ cladding mode, and (b) same for $LP_{0,41}$ and $LP_{0,42}$ cladding mode.

symmetric cladding modes is also being given in the supplementary document. The numerically computed spectrum of FBG with the surrounding medium of air and water is being given in Fig. S2. in supplementary document. The higher-order cladding mode possesses higher sensitivity and can be observed in the simulated spectrum. To compare the behavior of mode transition of comparative lower and higher-order cladding modes we have considered $LP_{0,11}$, $LP_{0,12}$ and $LP_{0,41}$, and $LP_{0,42}$ cladding modes. The four-layer cross-sectional model of FBG has been used for the computation purpose (core-clad-overlay-surrounding medium). The RI of the overlay was selected as $\sim$1.7, which is the RI of standard silica-based sol-gel materials. Fig. 4(a) shows the mode transition of $LP_{0,11}$ and $LP_{0,12}$ cladding mode and it can be understood that a sharp change of effective index is being observed after a certain thickness of the overlay. The Q point is the middle portion of the curve where the slope of the graph is best. In the case of $LP_{0,12}$ cladding mode, the Q-point for overlay RI 1.7 is nearly at $\sim$150 nm of the thickness of overlay. Intermodal separation between $LP_{0,11}$ and $LP_{0,12}$ cladding mode is $\sim$0.3 nm, it has been observed that in the case of $LP_{0,41}$ and $LP_{0,42}$ cladding modes the curve is steeper from the very beginning of the deposited thickness of overlay. The slope region can be divided into six portions (a, b, c, d, e, f, g, and h). The detail of slopes of each region of the cladding modes of FBG are being given in Tab.1s in the supplementary document.

It is being observed that the best slope is observed in portion 'a' of the Fig. 4(b) in case of comparative higher-order cladding mode $LP_{0,42}$. The slope of this portion is $\sim$[119.39 $\times$ 10^{-7}/nm of overlay] (within a thickness range of 0-100 nm) which is higher than the slope of the best region of $LP_{0,12}$ cladding mode which is $\sim$[37.24x10^{-7}/nm of overlay] near @ 150 nm of the thickness (120–180 nm thickness range). This result shows the conventional MT concept [14]–[16] of higher-order cladding mode is differ in a major way than comparative lower-order cladding modes. To characterize the detail effect of mode transition, variation of effective index with the thickness of the overlay has been computed for the number of modes (LP_{06}-LP_{07}, $LP_{0,11}$-$LP_{0,12}$, $LP_{0,16}$-$LP_{0,17}$, $LP_{0,21}$-$LP_{0,22}$, $LP_{0,26}$-$LP_{0,27}$, $LP_{0,31}$-$LP_{0,32}$, $LP_{0,36}$-$LP_{0,37}$, $LP_{0,41}$-$LP_{0,42}$,) and are being illustrated in Fig. S3 in the supplementary document. It is observed that after '$LP_{0,25}$' cladding mode the variation of effective indices with overlay thickness increases abruptly with thinner overlay layer and in case of $LP_{0,41}$-$LP_{0,42}$ cladding modes the slope is highest within the few tens of nm of overlay layer. The sensitivity of two lower-order cladding modes was experimentally studied before. Almost 10-fold of sensitivity enhancement was reported earlier with mode transition phenomena after a deposition of the polymeric overlay [15]. MT characteristics curve for $LP_{0,11}$/$LP_{0,12}$ and $LP_{0,41}$/$LP_{0,42}$ cladding modes are different so the scope and aim of the coating layers are also dissimilar in respective higher-order cladding modes. In the case of $LP_{0,42}$ cladding modes, a sharp change in effective index can be observed from the very beginning of the deposition of overlay. In the next phase of simulation, the rate of alteration of the effective index with a change in overlay thickness has been computed for two different cladding modes ($LP_{0,12}$ and $LP_{0,42}$ cladding mode)

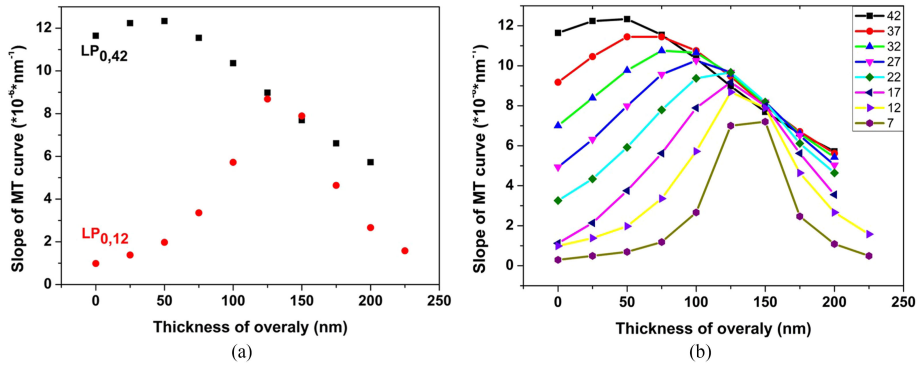

Fig. 5. (a) Variation of slope of MT characteristics curves for $LP_{0,12}$ and $LP_{0,42}$. (b) Characteristics of MT curve of other 8 cladding modes.

and is being shown in Fig. 5a. In Fig. 5b, slopes of 8 different cladding modes ($LP_{0,7}$, $LP_{0,12}$, $LP_{0,17}$, $LP_{0,22}$, $LP_{0,27}$, $LP_{0,32}$, $LP_{0,37}$ and $LP_{0,42}$) are being calculated within a narrow range of thickness (up to 225 nm). The variation of slopes of different cladding modes are being depicted clearly in Fig. 5b. It is prominent that the change of slope of MT curve of lower and comparative higher order cladding modes are dissimilar. A certain thickness is required to achieve the highest slope position for conventional lower order cladding modes (e.g., $LP_{0,12}$/$LP_{0,17}$/$LP_{0,22}$) and for higher-order cladding modes, the uppermost slope region is achievable within few tens of nanometers of overlay thickness and decreased exponentially with the thickness of overlay until to the region of second MT point.

The design strategy of optical fiber grating-based sensors with the effect of mode transition of cladding modes [15]–[17] needs to be optimized as per the order of the cladding modes because it has been observed that the MT behavior of comparative higher-order mode is different from that of lower-order cladding modes. It has been proved and reported earlier that the mode stretching effect can enhance the volume RI sensitivity of the lower-order cladding mode of FBG [26]. In this work, the effect of mode stretching on add-layer sensitivity of cladding modes has been discussed elaborately. The intermodal separation of $LP_{0,41}$-$LP_{0,42}$ is ~2.6 nm and is significantly higher than $LP_{0,11}$-$LP_{0,12}$ cladding modes separation (~0.6 nm). The sensitivity of higher-order cladding modes can be enhanced significantly with mode stretching phenomena. The intermodal separation of cladding mode with original and reduced diameter fiber has been evaluated numerically and is being shown in Fig. 6. With the reduction of clad diameter up to ~20 μm the modal separation between $LP_{0,41}$ and $LP_{0,42}$ cladding mode was ~4 nm which is quite significant for FBG based system.

The volume RI sensitivity of $LP_{0,42}$ and $LP_{0,37}$ cladding mode was ~27,000 pm/RIU and ~22,400 pm/RIU respectively with a cladding diameter of ~125 μm and with a reduction of cladding diameter by ~20 μm the computed sensitivity was found to be ~33,000 pm/RIU and ~26,200 pm/RIU respectively. In this work, we put more emphasis to identify the add-layer sensitivity S_{th} and S_{LRI}.

In the next part of the work, a detail analysis of add-layer sensitivity has been given. Adsorption of the bio-analyte layer above the surface of the sensor can be quantified as deposition of protein in (gm/cm^2) of the surface with specific RI. The mass adsorption over the sensing head is depending strictly on the concentration of mother solution of protein and it has been quantified by QCM, ellipsometry, and surface plasmon based resonance sensors [18]–[20]. This adhesion of mass can be modeled as a thin layer with specific thickness and density and as a result, the deposited thickness of different bio-specimens was identified with measurands. Depending on nature, the concentration of bio-specimen few nm to few tens of nm bio-layer could be adsorbed over the surface. With this idea thickness of different bio-specimen like antigen-antibody in immunoassay-based experiments [27] Specific proteins [28], Bovine Serum Albumin (BSA) [29], etc. were identified by quantification

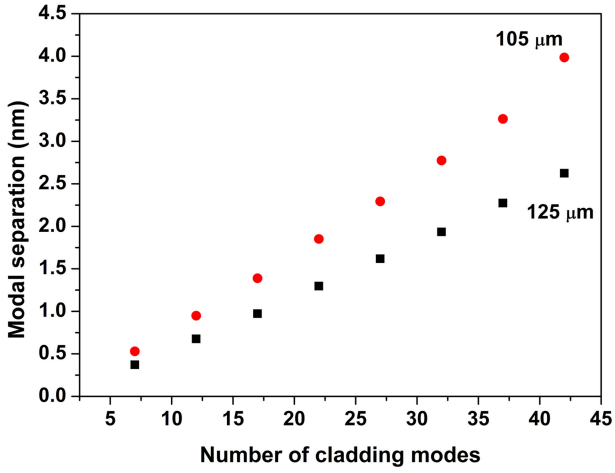

Fig. 6. Modal stretching of different order cladding modes with 125 μm and 105 μm of diameter of fiber for the different order of cladding mode.

of surface-based changes. FBG based biochemical sensors are used for the detection of different bio-specimen like specific immunoassay [30], Detection of Thrombin [31] and in many other applications [3], [13], [17], [33]. Add-layer sensitivity of cladding modes of FBG was computed with a six-layer model; namely core-clad-overlay-receptor-specimen layer- surrounding medium as shown in Fig. 1. The overlay RI has been kept constant to 1.7 as per standard Silica-Titania based sol-gel materials [34] and the receptor layer RI $\sim$ 1.5 for standard bio-functional polymer like Eudragit or polystyrene. The RI of target specimen layer has been kept constant at $\sim$1.6 [34], [35]. The thickness of receptor layer was chosen as $\sim$10 nm above the overlay surface. The overlay thickness for each of the cladding mode was considered different values as to utilize the maximum slope of the MT curve as shown in fig. 5b. Add-layer sensitivity is being calculated for different orders of cladding modes. It has been observed that add layer sensitivity is higher for high order of cladding mode, but for practical implementation, there is a limit, as writing of a very strong grating is case-specific and depends on fiber characteristics, so often index perturbation reaches to its maximum modulation strength, so we keep ourselves restricted up to $LP_{0,42}$ cladding mode. The value of add layer sensitivity at maximum suitable position has been calculated with the adhesion of $\sim$10 nm bio-analyte layer (RI $\sim$ 1.6) over the combined layer of overlay and $\sim$10 nm receptor layer. The add-layer sensitivity S_{th}, of the above-mentioned cladding modes, are computed numerically and has been given in Fig. 7a. Add-layer sensitivity S_{th} and S_{LRI} can be enhanced significantly with mode stretching. Add-layer sensitivity of different cladding modes with mode-stretching by reduction of 20 μm of fiber diameter has been shown in Fig. 7a. It is to be mentioned that surface RI sensitivity is another important measurand of distinct chemical and biological sensing applications. Surface RI sensitivity (S_{LRI}) has been measured with a change in RI of the receptor layer from 1.4 to 1.6. The thickness of the receptor layer was kept constant to be $\sim$20 nm for the entire simulation. The detection limit of surrounding RI is $\sim 4 \times 10^{-3}$ resolution with $LP_{0,42}$ cladding mode. The SLRI for different order of cladding mode has been computed and is shown in Fig. 7b. In the case of detection of the change in surface RI, sensitivity is not that significant but still can be used for the detection of gases like hydrogen, where a high percentage of RI change can occur in a sensitive Palladium layer [36]. After a detailed numerical computation, it can be shown that properly designed cladding modes of FBG possess enough sensitivity (S_{th}) for the detection of sub-nm adhesion of the target analyte layer over the surface. The add-layer sensitivity (S_{th} and S_{LRI}) can be increased with enhancement of RI of an overlay. The add-layer sensitivity (S_{th}) of $LP_{0,42}$ cladding mode with different overlay RI has been depicted in Fig. 8. With an overlay RI of $\sim$2, the add-layer sensitivity is $\sim$15 pm/nm attachment of analyte layer, this can be improved further with mode stretching, it

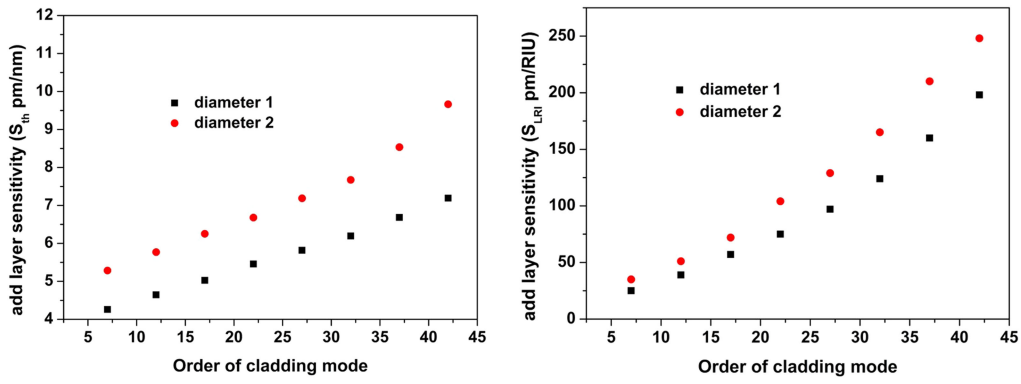

Fig. 7. Add layer sensitivity S_{th} and S_{LRI} of $LP_{0,42}$ cladding mode with two different diameters (diameter 1–125 μm, diameter 2–105 μm).

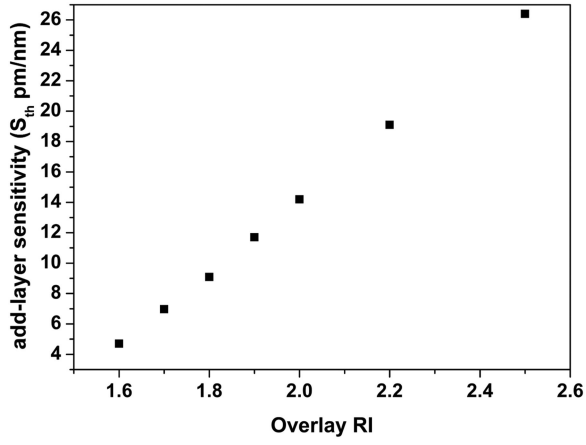

Fig. 8. Add-layer sensitivity S_{th} of $LP_{0,42}$ cladding mode with different values of overlay RI.

has been observed that with an overlay of RI ∼2 and mode stretching the add layer sensitivity can be ∼25 pm/nm attachment of bio-layer. The detailed analysis of surface RI sensitivity with a higher overlay layer is being accomplished and the mode transition curve of $LP_{0,42}$ with higher RI of overlay has been given in Fig. S4 in supplementary document. The add layer sensitivity (S_{th}) can be as high as ∼25 pm/nm attachment of analyte by an experimentally demonstrated overlay RI of ∼2 with tantalum oxide overlays [37]. With a standard interrogation technique 1 pm resolution change in resonance wavelength could be observed, so (1/25) = ∼ 0.04 nm or 40 pm attachment of target analyte could be detected with highly sensitive cladding mode of FBG.

4. Discussion & Conclusion

In this report, we have shown that with proper designing methodologies higher-order cladding mode of FBG can be used for volume and surface-based RI sensing applications. The spectrum of FBG has been simulated with a longer grating period rather than those used for the fabrication of FBGs in the telecommunication window near ∼1550 nm, as the cladding mode at higher wavelength provides higher sensitivity. Then a very strong FBG has been considered (with high index modulation) for further numerical computation, where a series of resonance bands of

symmetric cladding modes are found in the computed spectrum. 45 cladding modes are being observed in the spectrum. Then MT phenomena were studied extensively for almost each of the cladding modes. First, it has been observed that transition phenomena of higher-order cladding mode $LP_{0,41}$ and $LP_{0,42}$ are completely different from $LP_{0,11}$ and $LP_{0,12}$ and it has been concluded that the phenomena of variation of effective indices of cladding mode is different in comparative higher-order cladding mode (especially after '$LP_{0,25}$' cladding mode). The higher-order cladding modes in the FBG have two significant advantages for RI sensing: a) few tens of nm in thickness of overlay layer ($\sim$20 nm/with overlay RI $\sim$ 1.7 for $LP_{0,42}$) is enough to operate at maximum sensitive position for biological applications whereas in case of lower-order cladding modes a certain thickness ($\sim$150 nm/with overlay RI $\sim$ 1.7 for $LP_{0,12}$) is being required to reach the maximum sensitive position, b) broad linear region of operation is achievable for higher-order cladding mode ($\sim$120 nm for $LP_{0,42}$ cladding mode and $\sim$60 nm for $LP_{0,12}$ cladding mode), so dynamic range of the sensors with these higher-order modes is significantly higher than the dynamic range of lower-order cladding modes. In summary, the higher-order cladding mode (higher than $LP_{0,42}$) can provide higher sensitivity and better dynamic range but it requires a very strong FBG to utilize that specific higher-order cladding modes and fabrication of very strong FBG is not easy. Normally there are two ways of writing of a strong FBG. One of them is to use a high index modulation (spectrum of FBG with different index modulation is already given in supplementary document) but there is a trade-off as index modulation can't be increased indefinitely as per the material properties of the glass. With standard index modulation of $\sim$0.0005, the transmission loss of $LP_{0,42}$ is $\sim$2.5 dB, which is quite good enough for further use. The second way to write a strong grating is to enhance the length of the grating region with a moderate modulation index, but working with very long length FBG is not very convenient, so during fabrication optimal design scheme will be required to use comparative higher order cladding modes. Concept of mode stretching was incorporated to enhance sensitivity further, modal separation in terms of resonance wavelength separation of cladding modes of $LP_{0,11}$ and $LP_{0,12}$ was $\sim$0.6 nm with a radius $\sim$62.5 μm and it is found to be $\sim$0.82 nm with a radius of $\sim$52.5 μm, in case of $LP_{0,41}$ and $LP_{0,42}$ cladding mode it was respectively $\sim$2.6 nm and $\sim$3.92 nm respectively. The add layer sensitivity (S_{th} and S_{LRI}) has been computed for cladding modes of FBG for the first time to the best of our knowledge. A detail computation reveals the add-layer sensitivity of respective cladding mode can be as high as $\sim$40 pm/nm attachment of target analyte. With a modern spectrum analyzer resonance wavelength shift of $\sim$1 pm is easily observable. Sub-nm attachment of bio-analyte can be detected with help of symmetric cladding mode of FBG which would be very promising for this family of sensors. Quantification of bio-analytes or bio-chemical specimens normally determine with ellipsometer/QCM/SPR/SAW-based sensors, here it has been illustrated that with proper designing FBG can be used to measure surface-based changes during specific biological and chemical applications. The concept of higher-order mode reorganization with deposited overlay (especially modes higher than $LP_{0,25}$) leads to a new avenue of designing of the sensors where the sensors can be readily used for surface-based applications and only a thin layer ($\sim$few tens of nm) of overlay is require to be deposited. The fabrication of the device will be challenging as higher index of modulation can lead to the region of higher non-linearity of operation of the device. Type of the fiber, constituent materials of the fibers will be another important aspect to fabricate higher order cladding modes of FBG. Parameters like laser wavelength (for the inscription of grating), laser power, length of the fabricated grating are also need to be optimized as still there is no experimental demonstration for a meaningful generation of higher-order cladding modes for FBG. Apart from that the instruments to measure $\sim$1 pm wavelength shift is very costly so during fabrication of the device few critical issues have to be faced for proper use of higher symmetric order cladding mode based FBG sensors. In spite of complexities, fabrication of these sensors will add some additional advantages than conventional TFBGs as the spectrum of FBG with symmetric cladding mode is much clear than TFBG and cleanness of the spectrum will be useful in case of multiplexing of the sensors. The main Bragg peak always remains at the initial position as it is not influenced by the surrounding medium so it can be used as a temperature compensator as it is influenced only by a change of surrounding temperature and strain. With keeping this advantage in mind, self-temperature compensated biochemical sensing systems can be developed for specific

applications which are not possible for standalone FBG, TGBG or LPFG sensors. The behavior of comparative higher order cladding modes could be explored in the future for designing and fabrication of other grating-based sensors with LPFG, TFBG or different cascaded grating sensors for selective chemical or biological applications.

References

[1] F. Chiavaioli, F. Baldini, S. Tombelli, C. Trono, and A. Giannetti, "Biosensing with optical fiber gratings," *Nanophotonics*, vol. 6, pp. 663–679, 2017.

[2] X.-D. Wang and O. S. Wolfbeis, "Fiber optic chemical sensors and biosensors (2013–2015)," *Analytical Chemistry*, vol. 88, pp. 203–227, 2016.

[3] J. Albert, L. Shao, and C. Caucheteur, "Tilted fiber bragg grating sensors," *Laser Photon. Rev.*, vol. 7, pp. 83–108, 2013.

[4] T. Erdogan, "Fiber grating spectra," *IEEE J. Lightw. Technol.*, vol. 15, no. 8, pp. 1277–1293, Aug. 1997.

[5] A. Asseh, S. Sandgren, H. Ahlfeldt, B. Sahlgren, R. Stubbe, and G. Edwall, "Fiber optical Bragg grating refractometer," *Fiber Integr. Opt.*, vol. 17, pp. 51–62, 1998.

[6] K. Zhou, X. Chen, L. Zhang, and I. Bennion, "High-sensitivity optical chemsensor based on etched D-fibre Bragg gratings," *Electron. Lett.*, vol. 40, no. 4, pp. 232–234, 2004.

[7] W. Liang, Y. Huang, Y. Xu, R. K. Lee, and A. Yariv, "Highly sensitive fiber Bragg grating refractive index sensors," *Appl. Phys. Lett.*, vol. 86, no. 15, pp. 151122-1–151122-3, Apr. 2005.

[8] M. Giordano, M. Russo, A. Cusano, A. Cutolo, G. Mensitieri, and L. Nicolais, "Optical sensor mbased on ultrathin films of -form syndiotactic polystyrene for fast and high-resolution detection of chloroform," *Appl. Phys. Lett.*, vol. 85, pp. 5349–5351, 2004.

[9] T. Guo, A. Gonzalez-Vila, M. Loyez, and C. Caucheteur, "Plasmonic optical fiber grating immunosensing: A review," *Sensors, MDPI*, vol. 17, pp. 732–752, 2017.

[10] X Chen *et al.*, " Real-time detection of DNA interactions with long period fiber-grating-based biosensor," *Opt. Lett.*, vol. 32, pp. 2541–2543, 2007.

[11] J Yanga *et al.*, "Heavy metal ions probe with relative measurement of fiber Bragg grating," *Sensor Actuator B*, vol. 230, pp. 353–358, 2016.

[12] S. Sridevi, K. S. Vasu, N. Bhat, S. Asokan, and A. K. Sood, "Ultra sensitiveNO2 gas detection using the reduced graphene oxide coated etched fiber Bragg gratings," *Sensor Actuator B*, vol. 223, pp. 481–487, 2016.

[13] G. Laffont and P. Ferdinand, "Tilted short-period fibre- Bragg-grating-induced coupling to cladding modes for accurate refractometry," *Meas. Sci. Technol.*, vol. 12, pp. 765–770, 2001.

[14] Z. Li, X. Shen, Y. Hua, and X. Ruan, and Y. Dai, "Leaky mode transition and enhanced resonance in tilted fiber Bragg grating," *J. Appl. Phys.*, vol. 126, pp. 154501/0–154501/11, 2019.

[15] I. D. Villar, "Ultrahigh-sensitivity sensors based on thin-film coated long period gratings with reduced diameter, in transition mode and near the dispersion turning point," *Opt. Express*, vol. 23, pp. 8389–8398, 2015.

[16] I. D. Villar, M. Achaerandio, I. R. Matias, and Francisco, "Optimization of sensitivity in long period fiber gratings with overlay deposition," *Opt. Express*, vol. 13, pp. 56–68, 2004.

[17] S. Bandyopadhyay, T. K. Dey, N. Basumallick, P. Biswas, K. Dasgupta, and S. Bandyopadhyay, "High sensitive refractometric sensor using symmetric cladding modes of an FBG operating at mode transition," *IEEE J. Lightw. Technol.*, vol. 34, no. 14, pp. 3348–3353, Jul. 2016.

[18] P. Kvasnicka and J. Homola, "Optical sensors based on spectroscopy of localized surface plasmons on metallic nanoparticles: sensitivity considerations," *Biointerphases*, vol. 3, pp. FD4–FD11, 2008.

[19] C. G. Marxer, M. C. Coen, and L. Schlapbach, "Study of adsorption and viscoelastic properties of proteins with a quartz crystal microbalance by measuring the oscillation amplitude," *J. Colloid Interface Sci.*, vol. 261, pp. 291–298, 2003.

[20] C. Zhou *et al.*, "Human immunoglobulin adsorption investigated by means of quartz crystal microbalance dissipation, atomic force microscopy, surface acoustic wave, and surface plasmon resonance techniques," *Langmuir*, vol. 20, pp. 5870–5878, 2004.

[21] S. Bandyopadhyay, I. D. Villar, P. Biswas, N. Basumallick, T. K. Dey, and S. Bandyopadhyay, "Long period fiber grating for biosensing: An improved design methodology to enhance add-layer sensitivity," *IEEE J. Lightw. Technol.*, vol. 36, no. 4, pp. 1178–1184, Feb. 2018.

[22] S Bandyopadhyay *et al.*, "Long-period fiber grating: A specific design for biosensing applications," *Appl. Opt.*, vol. 56, pp. 9846–9854, 2017.

[23] E. Anemogiannis, E. N. Glytsis, and T. K. Gaylord, "Transmission characteristics of long-period fiber gratings having arbitrary azimuthal/radial refractive index variations," *IEEE J. Lightw. Technol.*, vol. 21, no. 1, pp. 218–227, Jan. 2003.

[24] T. Erdogan and J. Sipe, "Cladding-mode resonances in short- and long period fiber grating filters," *J. Opt. Soc. Amer.*, vol. 14, pp. 1760–1773, 1997.

[25] Y. Koyamada, "Numerical analysis of core-mode to radiation-mode coupling in long-period fiber gratings," *IEEE Photon. Technol. Lett.*, vol. 13, no. 4, pp. 308–310, Apr. 2001.

[26] A. Bahattacharya, M. Gangopadhyay, and S. Bandyopadhyay, "Designing of highly sensitive fiber bragg grating based volume refractive index sensors for biochemical applications," in *Proc. IEEE 9th Annu. Inf. Technol., Electron. Mobile Commun. Conf. (IEMCON)*, Vancouver, Canada, 2018, pp. 918–923.

[27] D. C. Culle, R. G. W. Brown, and C. R. Lowe "Detection of Immune-complex formation via surface plasmon resonance on gold-coated diffraction gratings," *Biosensors*, vol. 3, no. 4, pp. 1987–1988, pp. 211–225, 1987.

[28] F. Hook, B. Kasemo, T. Nylander, C. Fant, and K S. H. Elwing, "Variations in coupled water, viscoelastic properties, and film thickness of a Mefp-1 protein film during adsorption and cross-linking: A quartz crystal microbalance with dissipation monitoring, ellipsometry, and surface plasmon resonance study," *Analytical Chemistry*, vol. 73, pp. 5796–5804, 2001.
[29] E Wassel *et al.*, "Thickness dependence of bovine serum albumin adsorption on thin thermo responsive poly(diethylene glycol) Methyl ether methacrylate brushes by surface plasmon resonance measurements," *Langmuir*, vol. 32, pp. 9360–9370, 2016.
[30] L. S. Jung, C. T. Campbell, T. M. Chinowsky, M. N. Mar, and S. S. Yee, "Quantitative interpretation of the response of surface plasmon resonance sensors to adsorbed films," *Langmuir*, vol. 14, pp. 5636–5648, 1998.
[31] Q. Wang, J. Y. Jing, and B. Wang, "Highly sensitive SPR biosensor based on graphene oxide and staphylococcal protein a Co-modified TFBG for human IgG detection," *IEEE Trans. Instrum. Meas.*, vol. 68, no. 9, pp. 3350–3357, Sep. 2019.
[32] J. Lao *et al.*, "Gold nanoparticle-functionalized surface plasmon resonance optical fiber biosensor: In situ detection of thrombin with 1 n·M detection limit," *IEEE J. Lightw. Technol.*, vol. 37, no. 11, pp. 2748–2755, Jun. 2019.
[33] J. Janting, J. K. M. Pedersen, R. Inglev, G. Woyessa, K. Nielsen, and O. Bang, "Effects of solvent etching on PMMA microstructured optical fiber bragg grating," *IEEE J. Lightw. Technol.*, vol. 37, no. 18, pp. 4069–4079, Sep. 2019.
[34] F. Chiavaioli *et al.*, "Sol−Gel-based titania−silica thin film overlay for long period fiber grating-based biosensors," *Analytical Chemistry*, vol. 87, pp. 12024–12031, 2015.
[35] F. Chiavaioli *et al.*, "Towards sensitive label-free immune-sensing by means of turn-around point long period fiber gratings," *Biosens. Bioelectron.*, vol. 60, pp. 305–310, 2014.
[36] N Basumallick *et al.*, "Design of palladium-coated long-period fiber grating for hydrogen sensing," *IEEE J. Lightw. Technol.*, vol. 34, no. 21, pp. 4912–4919, Nov. 2016.
[37] M. Piestrzynska *et al.*, "Ultrasensitive tantalum oxide nano-coated long period gratings for detection of various biological targets," *Biosens. Bioelect*, vol. 133, pp. 8–15, 2019.